CHEMISTRY OF MATERIALS

Article

pubs.acs.org/cm

Two-Dimensional Fully Conjugated Polymeric Photosensitizers for Advanced Photodynamic Therapy

Zhonghua Xiang,[†,‡,§,⊥] Lin Zhu,[∥,⊥] Lei Qi,[∥] Lu Yan,[∥] Yuhua Xue,[∥] Dan Wang,[†,‡] Jian-Feng Chen,[*,†] and Liming Dai[*,‡,§,∥]

[†]State Key Laboratory of Organic−Inorganic Composites, Beijing University of Chemical Technology, Beijing 100029, China

[‡]Energy Institute, BUCT-CWRU International Joint Laboratory, Beijing University of Chemical Technology, Beijing 100029, China

[§]Centre of Advanced Science and Engineering for Carbon (Case4Carbon), Department of Macromolecular Science and Engineering, Case Western Reserve University, 10900 Euclid Avenue, Cleveland, Ohio 44106, United States

[∥]Institute of Advanced Materials for Nano-Bio Applications, School of Ophthalmology & Optometry, Wenzhou Medical University, Wenzhou 325027, China

Supporting Information

ABSTRACT: Photodynamic therapy (PDT) is attractive for treatment of various cancers, with a high selectivity, minimal long-term effect, and excellent cosmetic appeal. Well water-dispersive photosensitizers with strong optical absorption within the tissue transparency window (700−1000 nm) are needed for efficient PDT. However, clinically used PDT agents based on oligomeric porphyrin units (e.g., protoporphyrin IX) are effective at 532 nm irradiation only. Herein, we synthesized a two-dimensional covalent organic polymer (COP) containing fully conjugated multiple porphyrin macrocycles with sulfonic acid side groups. The resultant COP-P-SO_3H is well water-dispersive, showing strong optical absorption within the desired therapeutic window and a high quantum yield of reactive oxygen species, especially singlet oxygen ($^1O_2$), for efficiently killing tumor cells upon near-infrared light irradiation. Our first-principles calculations revealed that the observed high yield $^1O_2$ resulted from the unique side-on parallel diatomic adsorption (Yeager mode) of triplet oxygen molecules on the highly conjugated porphyrin rings in the photoexcited COP-P-SO_3H.

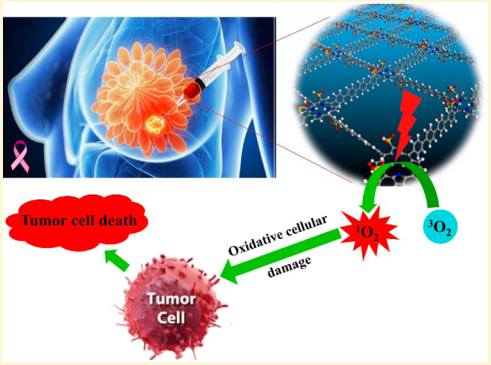

INTRODUCTION

Photodynamic therapy (PDT) has attracted tremendous attention as an emerging clinical modality for treatment of neoplastic and nonmalignant lesions, including cancers of the head and neck, brain, lung, pancreas, intraperitoneal cavity, breast, prostate, and skin, to name a few.[1−3] PDT generally involves photoexcitation of a photosensitizer, which transfers energy to surrounding O_2 to generate reactive oxygen species (ROS), especially singlet oxygen ($^1O_2$),[4] to impart a selective irreversible cytotoxic process to malignant cells with respect to noncancerous tissues. PDT with an optical precision could show a minimal toxicity to normal tissues, negligible systemic (organ) or long-term effect, and excellent cosmetic appeal. However, the near-infrared (NIR) light is often required to effectively penetrate biological tissues, such as skin and blood, with minimal normal tissue damage.[2,4] This is because visible light below 700 nm cannot penetrate deep into tissues with a high level of endogenous scatters and/or absorbers, such as oxy-/deoxy-hemoglobin, lipids, and water, in skin and blood.[5] Therefore, it is important to develop efficient photosensitizers with strong absorption in the desired therapeutic window (particularly, 700−1000 nm) for advanced PDT.

Porphyrin, a conjugated macrocycle with intense optical absorption, plays important roles in our life (e.g., in heme to act as a cofactor of the protein hemoglobin) and has been widely used as a photosensitizing reagent for PDT.[2] Due to the short conjugation length intrinsically associated with individual porphyrin macrocycles of a limited size, however, most of the clinically approved porphyrin-based photosensitizers show optical absorption well below 700 nm with insignificant absorption within the tissue transparency window (e.g., 700−900 nm)[2]. As a typical example, porfimer sodium (Photofrins), one of the widely used clinical PDT agents, with oligomeric porphyrin units being linked by *nonconjugated* ester and ether linkages to gain solubility, shows diminished absorption above 630 nm.[6] Therefore, it is highly desirable to develop new photosensitizers of a long conjugation length with alternating C−C single and C=C double bonds, and hence efficient absorption within the tissue transparency window (e.g., 700−900 nm). However, conjugated macromolecules without functionalization are poorly dispersive while functionalization

Received: August 28, 2016
Revised: October 30, 2016
Published: November 2, 2016

DOI: 10.1021/acs.chemmater.6b03619
Chem. Mater. 2016, 28, 8651−8658

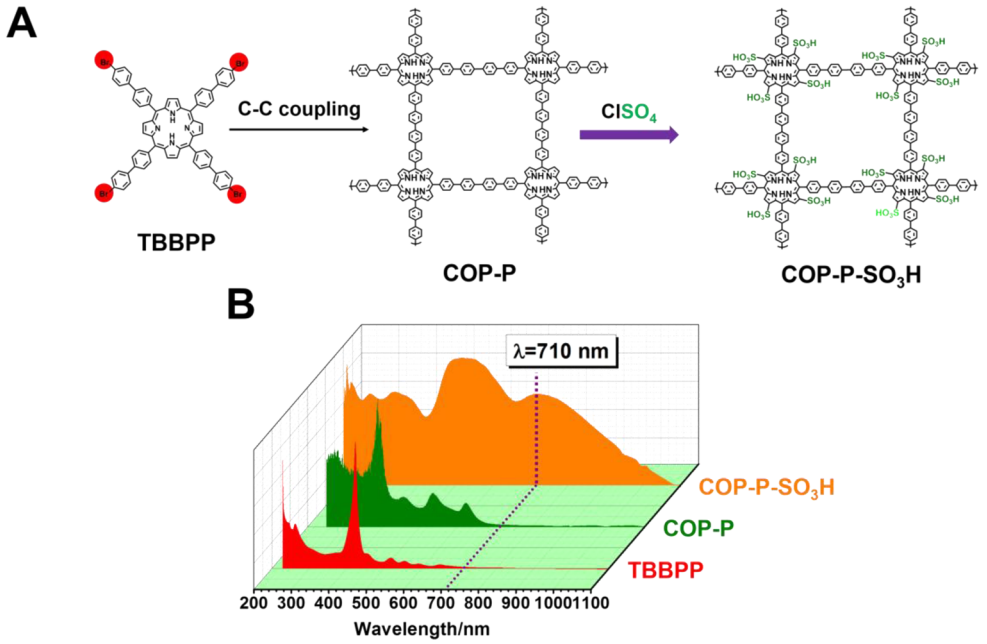

Figure 1. Synthesis and optical adsorption of sulfonated porphyrin-based covalent organic polymers. (A) Scheme for synthesis of COP-P-SO_3H. (B) UV−vis spectra of the aqueous solutions of COP-P-SO_3H, COP-P, and TBBPP (1 mg mL^{-1}).

often causes the conjugation length to be shortened and the optical adsorption to be reduced and blue-shifted. Therefore, it is still a big challenge to synthesize highly conjugated, but still well dispersive photosensitizers for advanced photodynamic therapy. Well water-dispersive highly conjugated photosensitizers, if realized, should hold great potential for various biomedical applications, including PDT. In this regard, we have recently synthesized a class of 2D covalent organic polymers (COPs) from various organic heterocycles, such as triazine, porphyrin, and their derivatives.[7−11] On this basis, we further synthesized in this study well *water-dispersive, fully conjugated* 2D COPs (i.e., COP-P-SO_3H, Figure 1A), in which multiple porphyrin macrocycles with sulfonic acid side groups are covalently bonded together through *conjugated* linkages. The resultant COP-P-SO_3H was demonstrated to be an efficient photosensitizer for breast cancer PDT. Compared with protoporphyrin IX (PPIX)—a benchmark PDT reagent that has been widely used in clinics with 532 nm irradiation, our newly developed water-dispersive and fully conjugated COP-P-SO_3H showed great potential for advanced PDT with a significantly high quantum yield of reactive oxygen species (ROS) for efficiently killing tumor cells upon NIR irradiation within the desired therapeutic window. The introduction of electron-rich sulfonic acid groups into the fully conjugated polymer backbone in COP-P-SO_3H was demonstrate to not only impart water-dispersibility but also reduce its band gap through both intramolecular charge-transfer and protonic doping (*vide infra*). The reduced band gap of COP-P-SO_3H led to significantly enhanced optical adsorption with a concomitant red-shift into the therapeutic window (up to 1100 nm, Figure 1B) for efficient PDT of breast and other cancer cells. Furthermore, it was found that the tumor cell viabilities significantly reduced with increasing COP-P-SO_3H concentration and irradiation time during the PDT process, through successive DNA damage due to an increased ROS generation. Our experimental results are complemented by the first-principles calculations, which revealed a photosensitization mechanism for the enhanced toxic singlet oxygen generation from the triplet oxygen molecules adsorbed on the highly conjugated porphyrin macrocycles in the side-on Yeager mode.[8]

As far as we are aware, COP-P-SO_3H is the first COP used for PDT, which for the first time allowed the PDT reagents based on porphyrin units (some of them have been widely used in clinics, such as PPIX) to be used with NIR light within the desired therapeutic window to dramatically enhance the PDT efficiency. Therefore, this work clearly indicates great potential of 2D COPs for exciting new applications, including PDT, along with their widespread uses for gas storage, catalysis, and optoelectronics.[12] The methodology developed in this study could be applied to the design and development of various 2D COPs for advanced PDT and beyond.

EXPERIMENTAL SECTION

Synthesis of COP-P. First, we synthesized COP-P from 4′-bromobiphenyl-4-ylporphyrin (TBBPP) via Ni(0)-catalyzed Yamamoto Ullmann cross-coupling reaction (Figure 1A).[8,11] Briefly, 1,5-cyclooctadiene (cod, 0.50 mL, 3.96 mmol) was added to a solution of bis(1,5-cyclooctadiene)nickel(0) ([$Ni(cod)_2$], 1.125 g, 4.09 mmol) and 2,2′-bipyridyl (0.640 g, 4.09 mmol) in dry DMF (65 mL), and the mixture was stirred until completely dissolved. 5,10,15,20-Tetrakis(4′-bromo-biphenyl-4-yl)porphyrin (TBBPP) (0.966 g, 0.785 mmol) was subsequently added to the resulting purple solution. Thereafter, the reaction vessel was heated at 85 °C overnight under a nitrogen atmosphere. After being cooled down to room temperature, 10 mL of concentrated HCl was added to the deep purple suspension, which would be changed into an aqua transparent solution. After filtration, the residue was washed with $CHCl_3$ (5 × 15 mL), THF (5 × 15 mL), and H_2O (5 × 15 mL), respectively, and dried in vacuum at 180 °C to give COP-P as cream powder (268 mg, 92% yield). Elemental analysis calcd (%) for $C_{68}H_{42}N_4$: C 89.25, H 4.63, N 6.12; found (%): C 88.76, H 4.55, N 5.68.

Synthesis of COP-P-SO_3H. COP-P was degassed at 200 °C for 24 h prior to use. Chlorosulfonic acid (4 mL) was added into 40 mL of dichloromethane solution containing 400 mg of degassed COP-P in an ice-bath. Thereafter, the resulting mixture was stirred at room temperature for 3 days. Then, the mixture was poured into ice, and

DOI: 10.1021/acs.chemmater.6b03619
Chem. Mater. 2016, 28, 8651−8658

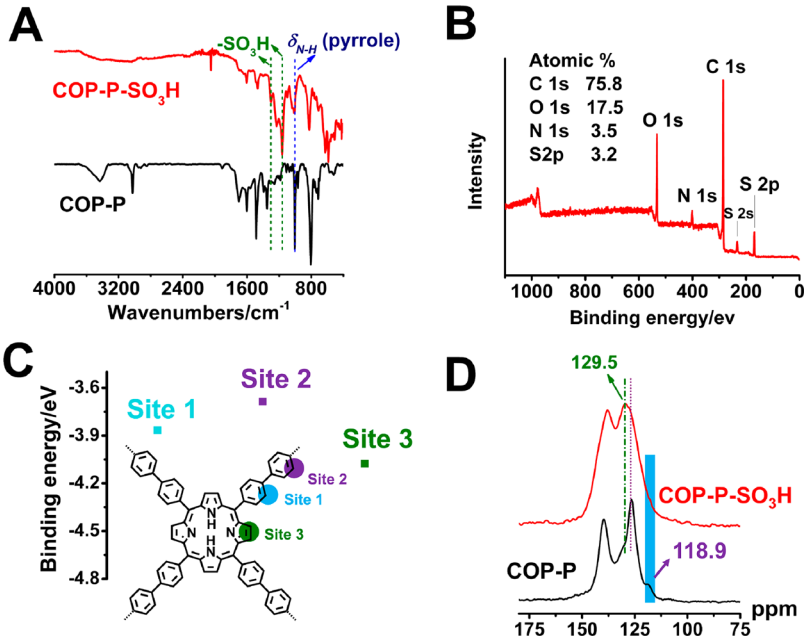

Figure 2. Characterization and photodynamic properties of COP-P-SO_3H. (A) FT-IR spectra of COP-P and COP-P-SO_3H. (B) XPS survey spectra for COP-P-SO_3H. (C) Adsorption binding energy for different position substitutions of sulfonic acid groups in COP-P-SO_3H. The corresponding molecule models for Sites 1, 2, and 3 are also included (cf. Figure S2). (D) ^{13}C CP/MAS spectra of COP-P-SO_3H, along with that of the unmodified COP-P for comparison.

solid was collected, washed with water substantially, and dried to produce COP-P-SO_3H as blue powder (532 mg).

Detection of reactive oxygen species (ROS) of COP-P-SO_3H. The generation of ROS was detected indirectly using 1,3-diphenylisobenzofuran (DPBF) as a chemical probe, whose absorbance would be diminished in the presence of ROS. Briefly, 50 μL of DPBF (1 mM) solution was added into 3 mL of COP-P-SO_3H solution (300 μg mL^{-1}). The mixed solution of DPBF and COP-P-SO_3H was then irradiated with 710 nm light, during which the absorption spectrum of the mixture was measured every 5 min.

RESULTS AND DISCUSSION

Synthesis and characterization of COP-P-SO_3H. COP-P was synthesized according to our previously reported procedure (Figure 1A, Method).[8,11] Through innovative design, we further performed sulfonation of COP-P with chlorosulfonic acid to produce *well dispersive* COP-P-SO_3H (Figure 1A, Method), which exhibited the desired strong adsorption into the NIR region (up to 1100 nm, Figure 1B) useful for PDT.

The reactions shown in Figure 1A were monitored by various spectroscopic measurements.[8] Figure 1B shows the UV−vis absorption spectra for TBBPP, COP-P, and COP-P-SO_3H. Compared with TBBPP and COP-P, the salient feature for COP-P-SO_3H is its strong adsorption above ~710 nm within the desired therapeutic window for PDT. The remarkable red-shift in optical adsorption from TBBPP through COP-P to COP-P-SO_3H seen in Figure 1B can be correlated to the corresponding band gap change shown in Figure S1 (cf. Table S1). The band gap energies listed in Table S1 are in a good agreement with the optical absorption edge wavelengths shown in Figure 1B, given that the electrochemical measurements often give a relatively low value for the band gap.[13] The introduction of electron-rich sulfonic acid groups reduced the band gap from 1.47 eV for COP-P to 1.07 eV for COP-P-SO_3H, indicating the band gap reduction caused by both intramolecular charge-transfer and protonic doping.[13] The reduced band gap of COP-P-SO_3H led to significantly enhanced optical adsorption within the therapeutic window (≥700 nm, Figure 1B) for efficient PDT (*vide infra*).

Upon sulfonation, two new peaks characteristic of the sulfonic group appeared at 1156 and 1312 cm^{-1} in the FTIR spectrum of COP-P-SO_3H (Figure 2A). The N−H peak at ~978 cm^{-1} was retained, implying the reservation of porphyrin ring skeletons during sulfonation with chlorosulfonic acid. Furthermore, the corresponding XPS survey spectrum of COP-P-SO_3H given in Figure 2B shows atomic percentages of 3.2%, 17.5%, 3.5%, and 75.8% for S, O, N, and C, respectively. The XPS atomic ratio of N/C ≈ 1:21 is close to the stoichiometric value of 1:17 for porphyrin. Moreover, the high-resolution XPS N 1s spectrum of COP-P-SO_3H (Figure S2) can be fitted into two different components corresponding to the pyrrolic N with H (397.7 eV) and pyrrolic N without H atom (399.8 eV),[14] respectively. The ratio of these two peak areas is close to 1:1, suggesting the structural integrity of porphyrin macrocycles was well reserved in COP-P-SO_3H, consistent with the FTIR data. The O/S ratio of 5.4 is higher than the stoichiometric ratio of 3, indicating the presence of physically adsorbed oxygen or water molecules.[8] On the other hand, the atomic ratio of N/S ≈ 1:1 suggests approximately four sulfonic acid groups have been introduced into one TBBPP monomer unit in COP-P-SO_3H (cf. Figure 1A).

To specify the substitution sites of sulfonic acid groups in COP-P-SO_3H, we calculated the charge distribution at the theoretical level of B3LYP/6-311g (2d, 2p) using the Gaussian 03 program,[15] and subsequently screening the active sites by sulfonation using the Vienna Atomic Simulation Package (VASP)[16] with the projector augmented wave (PAW) pseudopotentials[17] and the generalized gradient approximation of the Perdew, Burke, and Ernzernhof (PBE) function.[18] Three types of active sites were identified, localizing around the pyrrolic C and phenyl C atoms (shadowed by green, cyan, and purple circles in Figure S3), for sulfonation. Among them, the strongest binding site for sulfonation is the pyrrolic C, with a

DOI: 10.1021/acs.chemmater.6b03619
Chem. Mater. 2016, 28, 8651−8658

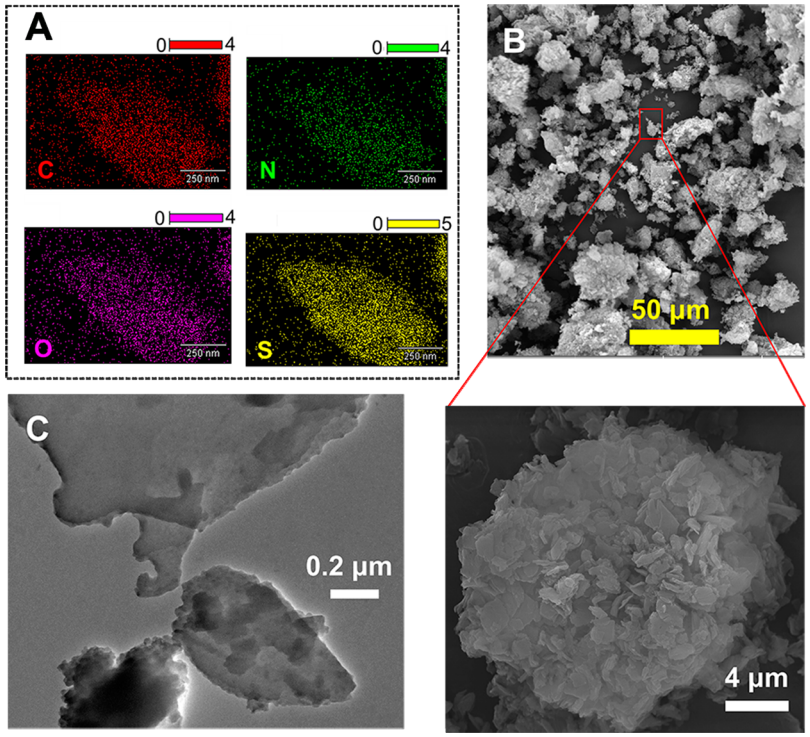

Figure 3. (A) Carbon, nitrogen, oxygen, and sulfur element mapping for the COP-P-SO_3H sample. (B) SEM images of the COP-P-SO_3H sample under different magnifications. (C) TEM image of the COP-P-SO_3H sample.

binding energy of −4.08 eV (Figure 2C). The above theoretical prediction was confirmed by our solid state ^{13}C NMR measurements (Figure 2D). As expected, COP-P shows three carbon peaks at 118.9, 126.5, and 139.6 ppm arising from the pyrrolic, phenyl, and methine bridge carbons, respectively.[11] Upon sulfonation, the pyrrolic carbon peak became very weak and a new peak at ∼129.5 ppm appeared, suggesting sulfonation along the pyrrolic ring. The absence of a peak characteristic of phenylsulfonic acid groups at >140 ppm implied that the sulfonic acid groups did not attach the phenyl rings in COP-P-SO_3H. Besides, the uniform distributions of S and O atoms seen in the TEM element mapping of COP-P-SO_3H (Figure 3A) indicate the occurrence of a uniform sulfonation of COP-P. These spectroscopic and microscopic results, together with the above theoretical prediction, suggest that the molecular structure shown in Figure 1A can be used as a working model for the COP-P-SO_3H, in which one H atom in each of the four pyrrolic rings within a porphyrin macrocycle was substituted by a sulfonic acid group.

The X-ray diffraction (XRD) profile for COP-P powder given in Figure S4 shows a strong diffraction peak at 21.3° corresponding to the π-stacking spacing (4.2 Å) between porphyrin macrocycles along the z-direction and another peak at 4.4° corresponding to the distance (20.1 Å) between the porphyrin rings connected through the phenyl groups in the plane. The disappearance of the peak at 3.9° after sulfonation is due, most probably, to some intraplane disorders caused by the introduction of $-SO_3H$ groups on the porphyrin rings. Although the XRD pattern revealed no long-range crystallographic order for COP-P-SO_3H, it still exhibited a layered microscopic morphology (Figures 3B and 3C), as is the case for the unmodified COP-P.[8]

Sulfonation significantly improved the hydrophilicity of the COP-P to impart water dispersibility to the resultant COP-P-SO_3H (Figure 4A), which is a desired feature for PDT. As seen in Figure 4B, the air−water contact angle was reduced from 107° for the COP-P to 0° for the COP-P-SO_3H.

***In vitro* PDT evaluation.** To investigate the PDT performance of COP-P-SO_3H, we first measured its ROS generation upon irradiation by using 1,3-diphenylisobenzofuran (DPBF) as a chemical probe.[19] As shown in Figure S5, the UV absorption peak at 418 nm characteristic of DPBF[16] showed a gradual decrease with time (Figure S5b) after incorporating 50

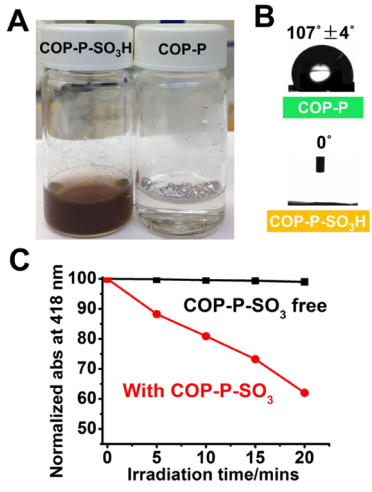

Figure 4. (A) Optical photos for aqueous dispersions (0.1 mg mL^{-1}) of COP-P and COP-SO_3H. (B) Contact angle images for COP-P and COP-P-SO_3H. (C) Normalized decay curves of the absorption density at 418 nm: the black line refers to the control experiment for a mixed solution of DPBF and COP-P-SO_3H without light irradiation, and the red line for DPBF in the presence of COP-P-SO_3H with light irradiation.

DOI: 10.1021/acs.chemmater.6b03619
Chem. Mater. 2016, 28, 8651−8658

μL of DPBF (1 mM) into 3 mL of an aqueous solution of COP-P-SO_3H (100 μg mL^{-1}) upon photoexcitation at 710 nm, whereas no obvious change was observed in a control experiment involving DPBF only without COP-P-SO_3H or their mixture without photoirradiation (Figure S5a, Figure 4C). These results clearly indicate the singlet oxygen generation from COP-P-SO_3H upon the NIR light irradiation.

To evaluate the cytotoxicity of the COP-P-SO_3H, we employed the MTT assay to determine the cell viability of the breast tumor cells (MDA-MD-231 cells) after having been irradiated with 710 nm light at a power of 5, 10, 15, and 20 min, respectively, in the presence of COP-P-SO_3H (50, 100, 150, and 200 μg mL^{-1}). Figure 5A shows no significant cell death

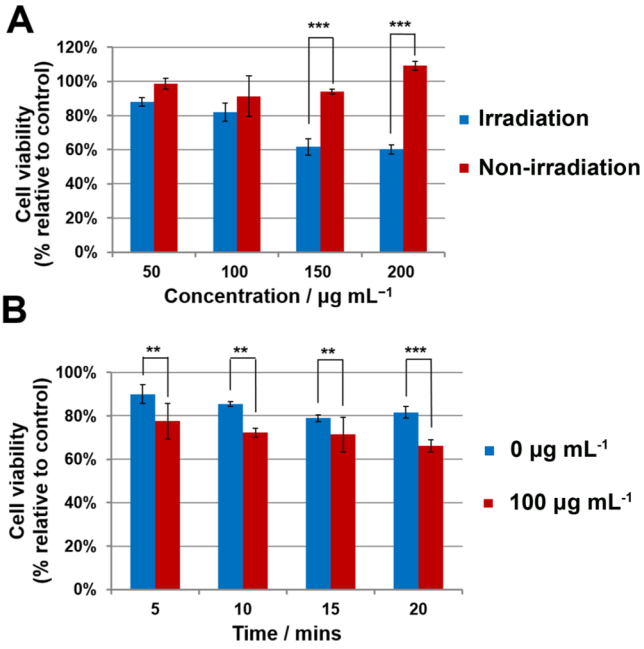

Figure 5. Cell viabilities of MDA-MD-231 cells studied by using the MTT method. (A) Cells were treated in cell culture media with COP-P-SO_3H photosensitizer at 50, 100, 150, and 200 μg mL^{-1} by exposure to a 710 nm laser for 10 min. (B) Cells were treated with and without COP-P-SO_3H photosensitizer by exposure to a 710 nm laser for 5, 10, 15, and 20 min, respectively. All the statistical results are obtained from the mean of at least three independent experiments. The symbol "*" denotes statistical significance (** $\leq$ 0.01, *** $\leq$ 0.001) compared with the negative control, and $p < 0.05$ was considered significant.

was observed in the presence of COP-P-SO_3H (50, 100, 150, and 200 μg mL^{-1}) without light irradiation, indicating low cytotoxicities for COP-P-SO_3H. However, the cell viabilities significantly decrease after the COP-P-SO_3H-induced PDT, showing a COP-P-SO_3H-concentration dependent (Figure 5A) and an irradiation-time dependent (Figures 5B) cell viability. Clearly, therefore, the death of tumor cells was caused by the photoinduced ROS generation from the COP-P-SO_3H photosensitizer.

The ROS generation by photoirradiation of COP-P-SO_3H was further monitored by using DCFH-DA as an ROS probe. Although DCFH-DA is nonfluorescent, its oxidized product (DCF) generated by reacting with ROS shows green fluorescence.[4] As expected, Figures 6A and 6B show an irradiation-time dependent (Figure 6A) and a COP-P-SO_3H-concentration (Figure 6B) dependent increase in the ROS from 1- to ~2-fold, respectively, while the ROS generation is negligible in the pure tumor cell system. Furthermore, a well-known clinically approved photosensitizer (*i.e.*, PPIX)[20,21] with a high singlet oxygen quantum yield (0.54–0.6)[22] was used as a reference[23] to determine the singlet oxygen quantum yield (ϕ_Δ) for COP-P-SO_3H. It was found that $\phi_{\Delta(\text{COP-P-SO}_3\text{H})}/\phi_{\Delta(PPIX)}$ equals 1.2, suggesting an even higher singlet oxygen quantum yield for COP-P-SO_3H (Figure S6). These results indicate the promising potential of COP-P-SO_3H as an efficient photosensitizer within the desired therapeutic window for advanced PDT.

Although Figure 5 shows a low cytotoxicity for COP-P-SO_3H without irradiation, we further evaluated the genotoxicity of COP-P-SO_3H, as various materials have been known to cause ROS-induced DNA damage, though they showed no serious cytotoxicity at the cell level.[24,25] To study the DNA damage of "live" cells potentially caused by the photogenerated ROS from COP-P-SO_3H under irradiation, we performed flow cytometry measurements on breast tumor cells (MDA-MD-231 cells) after COP-P-SO_3H mediated PDT. Four representative biomarkers, p53, OGG1, Rad51, and XRCC4, were used to monitor the DNA damage. The p53 is a tumor suppressor protein (53 kDa) that remains inactive under normal conditions and becomes active upon DNA damage caused by irradiation or oxidative stress.[25] Our results given in Figure 6F and Figure S7 show a remarkable increase in the p53 content from 0.92% to 4.29% after the COP-P-SO_3H-induced PDT. To determine the specific kinds of DNA damage induced by COP-P-SO_3H PDT, we examined the OGG1 expression, which is the major enzyme repairing 8-oxoguanine (8-oxoG): a mutagenic guanine base lesion caused by ROS.[24] As seen in Figure 6F, the COP-P-SO_3H-induced PDT significantly elevated the expression of OGG1 (18.54% compared with 0.86% for the control experiment), suggesting DNA damage through a mutagenic guanine base lesion. To examine the possible breakdown of the DNA double strand, we also investigated two key double strand break repair proteins: Rad51 (related with homologous recombination repair) and X-ray cross-complementation group 4 (XRCC4, involved in nonhomologous end join repair).[26] Figures 6C–F and Figure S7 clearly show the expression of Rad51 and XRCC4 occurred after the COP-P-SO_3H-induced PDT, indicating that the ROS generated during PDT with the COP-P-SO_3H photosensitizer could cause the breakdown of DNA double strains: an additional advantage for PDT. Although significant expressions of p53, OGG1, Rad51, and XRCC4 proteins have been observed in COP-P-SO_3-mediated tumor cells under irradiation, they are insignificant for the control experiments without irradiation (Figure 6F), indicating a low dark genotoxicity for a high photoselectivity.

Mechanism study on singlet oxygen generation. To study the mechanism of singlet oxygen generation from photoirradiation of COP-P-SO_3H, we performed the first-principles calculations with B3LYP hybrid density functional theory with the Gaussian program[15] based on the cluster model derived from the above experimental characterization data. Our calculations revealed that O_2 molecules prefer to adsorb via the Yeager model[12,27] (Figures S8–17 and Table S2) in COP-P-SO_3H and that the optimized O_2 adsorption site is on the top of the H-free pyrrolic N in the porphyrin ring (Figure S13). Furthermore, our molecular orbital calculations indicated that the HOMO is almost entirely localized in the porphyrin ring, being dominantly associated with the σ-bonding orbital from the pyrrolic N (No. 22 and No. 24 in Figure S18) and the π-

DOI: 10.1021/acs.chemmater.6b03619
Chem. Mater. 2016, 28, 8651–8658

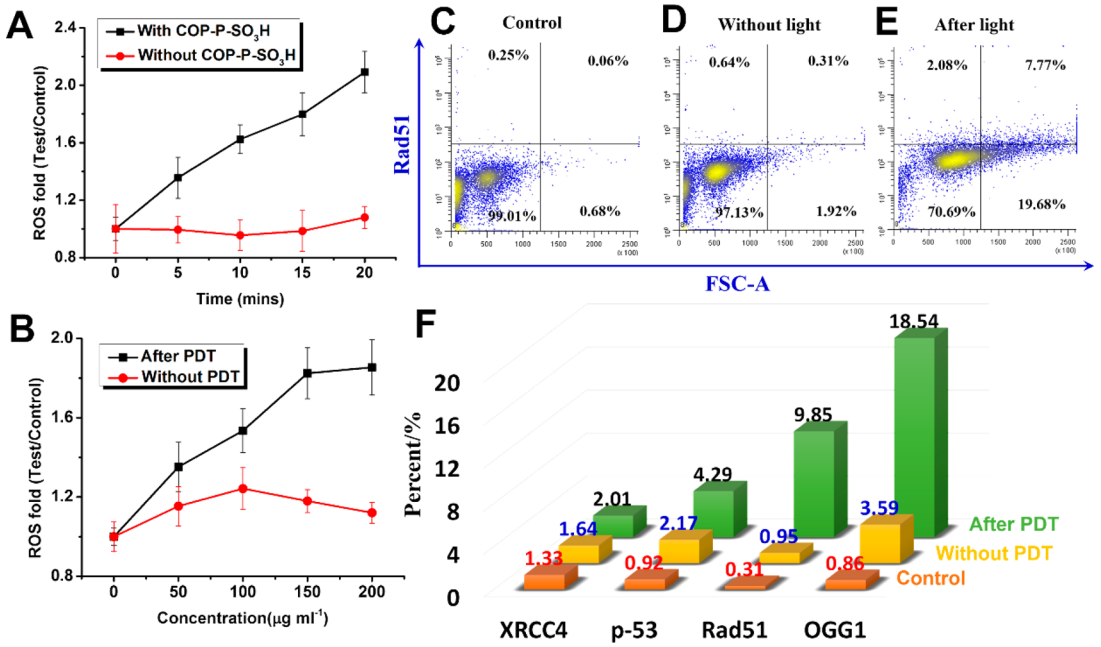

Figure 6. Induction effects of COP-P-SO_3H on DNA-damage. (A, B) The ROS generation assay in the tumor cell system. For comparison, the system without photosensitizer COP-P-SO_3H but with irradiation in part A and the system containing COP-P-SO_3H but without irradiation in part B were also included. (C–E) Rad51 protein expression derived from flow cytometric analyses of the (C) MDA-MD-231 cells without COP-P-SO_3H after irradiation at 710 nm light for 10 min, (D) MDA-MD-231 cells with COP-P-SO_3H, but without the light irradiation, and (E) MDA-MD-231 cells with COP-P-SO_3H after irradiation at 710 nm light for 10 min (concentration of COP-P-SO_3H: 150 μg mL^{-1}). Immunofluorescence staining Rad51 antibody was analyzed by flow cytometry. (F) COP-P-SO_3H induced XRCC4, p-53, Rad51, and OGG-1 protein expression. The numbers refer to the ratios of positive cells to total cells in % (cf. Figure 3C and Figure S14).

bonding orbital from the pyrrolic and methine bridge carbons in the porphyrin ring, while the LUMO is mainly associated with the σ-antibonding orbital from oxygen molecules and the π-antibonding orbital from the pyrrolic ring and the methine bridge carbon in the porphyrin (Figure 7A). Clearly, therefore, the charge density distribution calculations indicate that the electron was dominantly transferred from pyrrolic N (No. 24 in Figure S18) to an oxygen molecule when it approached the porphyrin ring (Figure S19).

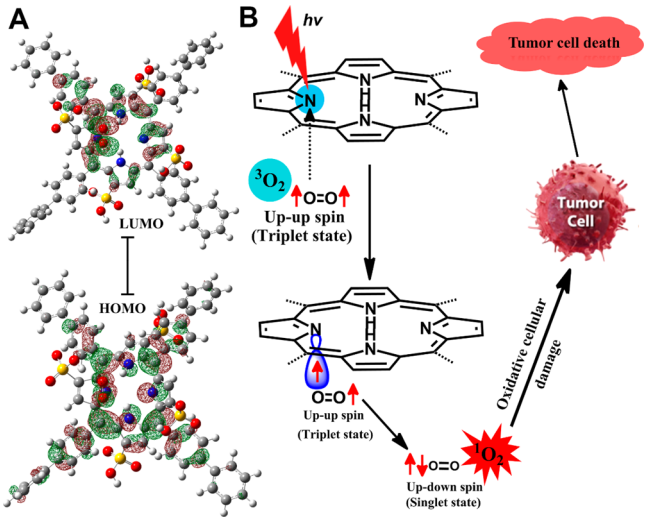

Figure 7. Mechanism for the generation of reactive oxygen species during the COP-P-SO_3H-induced PDT. (A) Contour plots of the HOMO and LUMO for O_2 adsorbed in the COP-P-SO_3H complex. The green and brown meshes indicate the orbitals in the different phases from one another. Colored balls indicate: C, gray; H, white; N, blue; S, yellow; and O, red. (B) Proposed mechanism for the COP-P-SO_3H-induced PDT.

The above results, along with those reported previously on the titanium(IV)–porphyrin,[28] are consistent with the following PDT process. As schematically shown in Figure 7B, the COP-P-SO_3H complex is turned from its ground state into the excited state upon NIR photoexcitation. Once the triplet oxygen approaches the N atoms (No. 24 in Figure S25) in the excited porphyrin ring, the molecular orbital overlapping promotes the energy transfer from the excited COP-P-SO_3H to triplet oxygen, followed by subsequent conversion of the spin direction from an up–up to an up–down spin state to form the toxic singlet oxygen $^1O_2$ for killing the tumor cells during the COP-P-SO_3H mediated PDT. In the meantime, the energy transfer from the excited COP-P-SO_3H to the triplet oxygen also facilitates the COP-P-SO_3H complex to return to its ground state for the next cycle of the singlet oxygen generation. Compared to the isolated porphyrin macrocycle (e.g., TBBPP), the much longer conjugation length in our newly developed 2D covalent organic polymers with multiple porphyrin macrocycles covalently bonded together through *conjugated* linkages (e.g., COP-P-SO_3H) could not only extend the absorption wavelength into the tissue transparency window (up to 1000 nm) but also enhance energy transfer between the photosensitizer and adsorbed oxygen under photoexcitation - both facilitate the efficient PDT.

CONCLUSION

In summary, we have, for the first time, developed a well water-dispersive, fully conjugated two-dimensional covalent organic polymer (i.e., COP-P-SO_3H) via a facile and scalable, but very efficient and cost-effective, Yamamoto Ullmann cross-coupling

DOI: 10.1021/acs.chemmater.6b03619
Chem. Mater. 2016, 28, 8651–8658

of multiple porphyrin macrocycles through conjugated linkages followed by sulfonation. The resultant COP-P-SO_3H of a good dispersiveness and low band gap exhibited strong optical absorption up to 1100 nm and acted as an efficient photosensitizer for advanced photodynamic therapy with a 20% higher singlet oxygen quantum yield than that of the clinically used protoporphyrin IX (PPIX), but a negligible cyto-/genotoxicity without light exposure. Compared to those isolated porphyrin macrocycles (e.g., PPIX, TBBPP), COP-P-SO_3H, with fully conjugated multiple porphyrin macrocycles, could effectively generate singlet oxygen species during the PDT process to efficiently kill the breast tumor cells (MDA-MD-231 cells) through successive DNA damage, as revealed by the combined experimental and theoretical approach used in this study. This is the first time for 2D covalent organic polymers (COPs) to be used as efficient photosensitizers of practical significance for advanced PDT. This work clearly opens up exciting new applications for COPs as well as new avenues for the development of other novel 2D COPs for advanced cancer therapy and beyond.

■ ASSOCIATED CONTENT

Supporting Information

The Supporting Information is available free of charge on the ACS Publications website at DOI: 10.1021/acs.chemmater.6b03619.

Experimental procedures, theoretical calculations, analytical data, and PDT performance investigation (PDF)

■ AUTHOR INFORMATION

Corresponding Authors

*E-mail: chenjf@mail.buct.edu.cn.

*E-mail: lxd115@case.edu.

Author Contributions

⊥Z.X. and L.Z. contributed equally to this work.

Notes

The authors declare no competing financial interest.

■ ACKNOWLEDGMENTS

This work was supported by NSF of China (51502012; 21676020; 201620102007); The National Key Technology Support Program of China (2012BAC25B06); Beijing Natural Science Foundation (2162032); the Start-up fund for talent introduction of Beijing University of Chemical Technology; Talent cultivation of State Key Laboratory of Organic−Inorganic Composites; the Fundamental Research Funds for the Central Universities (ZY1508, BUCTRC201601), and the "111" project of China (B14004). This work is also partially supported by the open-funding program of State Key Laboratory of Organic−Inorganic Composites, Wenzhou Medical University (WMU-CWRU, SPN2330), NSF (CMMI-1400274), DOD-AFOSR-MURI (FA9550-12-1-0037), and Zhejiang National Nature Science Foundation (LQ14C100002). We are thankful to F. Huo, W. Zhang, D. Cheng, D. Cao, and W. Wang for some theoretical calculation assistance and helpful discussions on first-principles calculations.

■ REFERENCES

(1) Dolmans, D.; Fukumura, D.; Jain, R. K. Photodynamic Therapy for Cancer. *Nat. Rev. Cancer* **2003**, *3*, 380−387.

(2) Kamkaew, A.; Lim, S. H.; Lee, H. B.; Kiew, L. V.; Chung, L. Y.; Burgess, K. BODIPY Dyes in Photodynamic Therapy. *Chem. Soc. Rev.* **2013**, *42*, 77−88.

(3) Agostinis, P.; Berg, K.; Cengel, K. A.; Foster, T. H.; Girotti, A. W.; Gollnick, S. O.; Hahn, S. M.; Hamblin, M. R.; Juzeniene, A.; Kessel, D.; Korbelik, M.; Moan, J.; Mroz, P.; Nowis, D.; Piette, J.; Wilson, B. C.; Golab, J. Photodynamic Therapy of Cancer: An Update. *Ca-Cancer J. Clin.* **2011**, *61*, 250−281.

(4) Tian, J.; Ding, L.; Xu, H.-J.; Shen, Z.; Ju, H.; Jia, L.; Bao, L.; Yu, J.-S. Cell-Specific And Ph-Activatable Rubyrin-Loaded Nanoparticles for Highly Selective Near-Infrared Photodynamic Therapy Against Cancer. *J. Am. Chem. Soc.* **2013**, *135*, 18850−18858.

(5) Klohs, J.; Wunder, A.; Licha, K. Near-Infrared Fluorescent Probes for Imaging Vascular Pathophysiology. *Basic Res. Cardiol.* **2008**, *103*, 144−151.

(6) Lightdale, C. J.; Heier, S. K.; Marcon, N. E.; McCaughan, J. S.; Gerdes, H.; Overholt, B. F.; Sivak, M. V.; Stiegmann, G. V.; Nava, H. R. Photodynamic Therapy With Porfimer Sodium Versus Thermal Ablation Therapy with Nd-Yag Laser for Palliation of Esophageal Cancer - A Multicenter Randomized Trial. *Gastrointest. Endosc.* **1995**, *42*, 507−512.

(7) Xiang, Z. H.; Cao, D. P. Porous Covalent-Organic Materials: Synthesis, Clean Energy Application And Design. *J. Mater. Chem. A* **2013**, *1*, 2691−2718.

(8) Xiang, Z. H.; Cao, D. P.; Huang, L.; Shui, J. L.; Wang, M.; Dai, L. M. Nitrogen-Doped Holey Graphitic Carbon from 2D Covalent Organic Polymers for Oxygen Reduction. *Adv. Mater.* **2014**, *26*, 3315−3320.

(9) Xiang, Z. H.; Zhou, X.; Zhou, C. H.; Zhong, S.; He, X.; Qin, C. P.; Cao, D. P. Covalent-Organic Polymers for Carbon Dioxide Capture. *J. Mater. Chem.* **2012**, *22*, 22663−22669.

(10) Xiang, Z. H.; Cao, D. P.; Wang, W. C.; Yang, W. T.; Han, B. Y.; Lu, J. M. Postsynthetic Lithium Modification of Covalent-Organic Polymers for Enhancing Hydrogen And Carbon Dioxide Storage. *J. Phys. Chem. C* **2012**, *116*, 5974−5980.

(11) Xiang, Z. H.; Xue, Y. H.; Cao, D. P.; Huang, L.; Chen, J. F.; Dai, L. M. Highly-Efficient Electrocatalysts for Oxygen Reduction Based On 2D Covalent Organic Polymers Complexed with Non-Precious Metals. *Angew. Chem., Int. Ed.* **2014**, *53*, 2433−2437.

(12) Xiang, Z. H.; Cao, D. P.; Dai, L. M. Well-Defined Two Dimensional Covalent Organic Polymers: Rational Design, Controlled Syntheses, and Potential Applications. *Polym. Chem.* **2015**, *6*, 1896−1911.

(13) Dai, L. M. *Intelligent Macromolecules for Smart Devices*; Springer-Verlag: Berlin, 2004.

(14) Ghosh, A.; Fitzgerald, J.; Gassman, P. G.; Almlof, J. Electronic Distinction Between Porphyrins And Tetraazaporphyrins. Insights from X-Ray Photoelectron Spectra of Free Base Porphyrin, Porphyrazine, And Phthalocyanine Ligands. *Inorg. Chem.* **1994**, *33*, 6057−6060.

(15) Frisch, M. J.; Trucks, G. W.; Schlegel, H. B.; Scuseria, G. E.; Robb, M. A.; Cheeseman, J. R.; Montgomery, J. A., Jr.; Vreven, T.; Kudin, K. N.; Burant, J. C. *Gaussian 03*, Revision C.02; Gaussian, Inc.: Wallingford, CT, 2004.

(16) Kresse, G.; Furthmüller, J. Efficient iterative schemes for ab initio total-energy calculations using a plane-wave basis set. *Phys. Rev. B: Condens. Matter Mater. Phys.* **1996**, *54*, 11169.

(17) Blöchl, P. E. Projector augmented-wave method. *Phys. Rev. B: Condens. Matter Mater. Phys.* **1994**, *50*, 17953.

(18) Perdew, J. P.; Burke, K.; Ernzerhof, M. Generalized gradient approximation made simple. *Phys. Rev. Lett.* **1996**, *77*, 3865.

(19) Qian, J.; Gharibi, A.; He, S. L. Colloidal Mesoporous Silica Nanoparticles with Protoporphyrin IX Encapsulated for Photodynamic Therapy. *J. Biomed. Opt.* **2009**, *14*, 014012.

(20) Peng, Q.; Berg, K.; Moan, J.; Kongshaug, M.; Nesland, J. M. 5-Aminolevulinic Acid-Based Photodynamic Therapy: Principles And Experimental Research. *Photochem. Photobiol.* **1997**, *65*, 235−251.

(21) Peng, Q.; Warloe, T.; Berg, K.; Moan, J.; Kongshaug, M.; Giercksky, K. E.; Nesland, J. M. 5-Aminolevulinic Acid-Based

DOI: 10.1021/acs.chemmater.6b03619
Chem. Mater. 2016, 28, 8651−8658

Photodynamic Therapy - Clinical Research And Future Challenges. *Cancer* **1997**, *79*, 2282−2308.
(22) Fernandez, J. M.; Bilgin, M. D.; Grossweiner, L. I. Singlet Oxygen Generation by Photodynamic Agents. *J. Photochem. Photobiol., B* **1997**, *37*, 131−140.
(23) Zhang, Y.; Qian, J.; Wang, D.; Wang, Y. L.; He, S. L. Multifunctional Gold Nanorods with Ultrahigh Stability And Tunability for *In Vivo* Fluorescence Imaging, Sers Detection, And Photodynamic Therapy. *Angew. Chem., Int. Ed.* **2013**, *52*, 1148−1151.
(24) Zhu, L.; Chang, D. W.; Dai, L. M.; Hong, Y. L. DNA Damage Induced by Multiwalled Carbon Nanotubes in Mouse Embryonic Stem Cells. *Nano Lett.* **2007**, *7*, 3592−3597.
(25) Xing, Y.; Xiong, W.; Zhu, L.; Osawa, E.; Hussin, S.; Dai, L. M. DNA Damage in Embryonic Stem Cells Caused by Nanodiamonds. *ACS Nano* **2011**, *5*, 2376−2384.
(26) Hoeijmakers, J. H. J. Genome Maintenance Mechanisms for Preventing Cancer. *Nature* **2001**, *411*, 366−374.
(27) Shi, Z.; Zhang, J. J.; Liu, Z. S.; Wang, H. J.; Wilkinson, D. P. Current Status of Ab Initio Quantum Chemistry Study for Oxygen Electroreduction on Fuel Cell Catalysts. *Electrochim. Acta* **2006**, *51*, 1905−1916.
(28) Matsumoto, T.; Takamura, K. Photo-Excitation Energy Transfer Between a Titanium(IV)-Porphyrin Complex And Oxygen Molecule. *Anal. Methods* **2012**, *4*, 4289−4294.

DOI: 10.1021/acs.chemmater.6b03619
Chem. Mater. 2016, 28, 8651−8658